minerals

MDPI

Article

Identification of Some Gem Quality Blue to Green Li-Tourmalines

Lorenzo Pasetti [1,*], Laura Borromeo [2], Danilo Bersani [1], Sergio Andò [2], Jurgen Schnellrath [3], Ugo Hennebois [4] and Stefanos Karampelas [4]

[1] Department of Mathematical, Physical and Computer Sciences, University of Parma, 43124 Parma, Italy; danilo.bersani@unipr.it
[2] Laboratory for Provenance Studies, Department of Earth and Environmental Sciences, University of Milano-Bicocca, 20126 Milan, Italy; laura.borromeo@unimib.it (L.B.); sergio.ando@unimib.it (S.A.)
[3] Centro de Tecnologia Mineral—Centre for Mineral Technology, Rio de Janeiro 21941-908, Brazil; jurgen@cetem.gov.br
[4] Laboratoire Français de Gemmologie (LFG), 75009 Paris, France
* Correspondence: lorenzo.pasetti@unipr.it

Abstract: Due to their appealing colors, gem quality tourmalines, particularly the blue to green Cu- and Mn-bearing Li-tourmalines known as the Paraíba type, have been of significant interest since their discovery at the end of 1980s. At the same time, the demand of other similar colored tourmalines increased. Most Paraíba-type tourmalines belong to the elbaite species; however, liddicoatite gems can also be found. Recognizing and classifying various tourmaline species, especially these valued Paraíba-type tourmalines, are important for geologists, mineralogists, mineral collectors, and gemologists. This study explores the application of Raman spectroscopy in random crystal orientations to distinguish between the elbaite and liddicoatite tourmaline species. Raman spectra were collected from faceted blue to green Li-tourmalines alongside chemical analysis using EDXRF (Energy Dispersive X-ray Fluorescence), UV-Vis-NIR (Ultraviolet-Visible-Near InfraRed Spectroscopy), and PL (Photoluminescence spectroscopy) to provide comprehensive characterization. The results show that Raman spectroscopy, particularly in the OH stretching region, is a useful tool for differentiating elbaite from liddicoatite, and this identification remains consistent regardless of crystal orientation. The fingerprint region in the Raman spectra, on the other hand, is orientation-dependent and can only differentiate the two species when detected in specific orientations. Furthermore, Paraíba-type tourmalines can be identified by visible-near infrared (Vis-NIR) spectroscopy, although not by Raman spectroscopy.

Keywords: tourmaline; Paraíba-type; elbaite; liddicoatite; Raman spectroscopy

Citation: Pasetti, L.; Borromeo, L.; Bersani, D.; Andò, S.; Schnellrath, J.; Hennebois, U.; Karampelas, S. Identification of Some Gem Quality Blue to Green Li-Tourmalines. *Minerals* **2024**, *14*, 44. https://doi.org/10.3390/min14010044

Academic Editor: Guanghai Shi

Received: 22 November 2023
Revised: 18 December 2023
Accepted: 25 December 2023
Published: 29 December 2023

1. Introduction

Tourmalines are a borosilicate mineral supergroup with a complicated chemical composition given by the general formula $XY_3Z_6(T_6O_{18})(BO_3)_3V_3W$, with each crystal site potentially occupied by the elements listed below [1]:

X site: Na^+, Ca^{2+}, □(vacant site), K^+.
Y site: Fe^{2+}, Mg^{2+}, Mn^{2+}, Al^{3+}, Li^+, Fe^{3+}, Cr^{3+}, Ti^{4+}, Zn^{2+}, Cu^{2+}, V^{3+}.
Z site: Al^{3+}, Fe^{3+}, Mg^{2+}, Fe^{2+}, Cr^{3+}, V^{3+}.
T site: Si^{4+}, Al^{3+}, B^{3+}.
B site: B^{3+}.
V site: $(OH)^-$, O^{2-}.
W site: F^-, $(OH)^-$, O^{2-}.

Gem quality tourmalines have gained increasing interest due to their variety of colors, caused by the presence of various transition elements, such as Fe^{2+}, Fe^{3+}, Mn^{2+}, Mn^{3+}, Ti^{4+}, Cu^{2+}, V^{3+} and Cr^{3+}, as well as color centers that are caused by radiation and act as chromophores [2]. Among all the different tourmaline varieties, blue to green tourmalines

are in high demand, with Cu- and Mn-bearing Li-tourmalines being the most sought-after. Paraíba-type tourmaline was named after the Brazilian state where it was first discovered at the end of the 1980s [3–5], even though other deposits were later found in other Brazilian regions, as well as in Nigeria and Mozambique [6,7]. Paraíba-type tourmalines consist primarily of elbaite (or fluor-elbaite, but simply mentioned as elbaite in the text), and secondly of liddicoatite (currently known as fluor-liddicoatite but simply mentioned as liddicoatite in the text); those from Mozambique have been included in this latter group [8–11]. No Paraíba-type tourmalines from rossmanite species are known to date [2]. Most of the gem-quality Paraíba-type tourmalines found in the market are heat treated [3,4,12,13]. Blue to green tourmalines, from the same species, without copper as principal colorants can also be found. Gem-quality deep green colored tourmalines from dravite-uvite species can also be encountered [2], but these are out of the scope of the present paper.

Identification of Li-tourmaline species, as well as other tourmaline species, is important for geologists, mineralogists, mineral collectors, and gemologists. Characterization might be achieved by using laser ablation inductively coupled plasma mass spectrometry (LA-ICP-MS) [14].

Raman spectroscopy has also been applied for tourmaline species characterization [15,16]. The main issue in the use of this method is related to the polarization effects [17–20]: the relative intensities of the Raman bands might differ in different crystallographic orientations. Thus, crystal orientation with respect to the polarization of incident light can highlight one type of vibrational mode over the other. In addition, with tourmalines being polar crystals, even some of the Raman band position can show a slight dependence on the orientation due to the LO-TO splitting effect [16]. The dependence of the Raman spectral parameters on the orientation might be an issue during the characterization of tourmalines, especially when mounted. In this paper, we tried to evaluate the applicability of Raman spectroscopy for the identification of randomly oriented blue to green Li-tourmalines and, more precisely, to discriminate elbaite from liddicoatite. For this purpose, fifteen faceted blue to green Li-tourmalines were thoroughly investigated by using Raman, UV-Vis-NIR (Ultraviolet-Visible-Near InfraRed), and PL (Photoluminescence) spectroscopies, while chemical characterization was achieved by using EDXRF (Energy Dispersive X-ray Fluorescence).

2. Materials and Methods

For this study, fifteen blue to green faceted Li-tourmalines from the Laboratoire Français de Gemmologie (LFG) reference collection were selected (Figure 1). The samples, their weight, dimensions, exact color, shape, cut, and geographic origin are presented in Table 1. The samples #0001, #0002, #0012, #0020, #0022, and #0063 are unheated, while the other nine samples are heated.

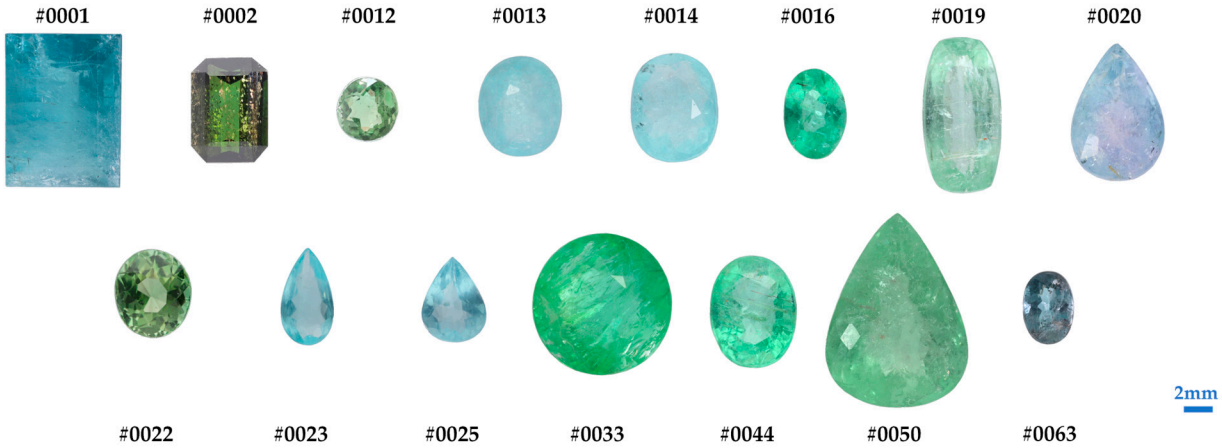

Figure 1. Images of the fifteen tourmaline gemstones analyzed in this work.

Table 1. List of tourmaline gemstones studied in this work with their main characteristics.

Sample	Provenance	Weight (ct)	Dimensions (mm)	Color	Shape-Cut
#0001	Nigeria	2.584	9.19 × 7.04 × 4.83	Greenish blue	Rectangular-Step
#0002	Brazil	0.738	6.32 × 4.65 × 2.97	Dark greyish green	Rectangular Corner Cut-Step
#0012	Nigeria	0.460	4.45 × 4.60 × 3.20	Yellowish green	Round-Brillant
#0013	Nigeria	0.746	6.01 × 4.88 × 3.51	Light greenish blue	Oval-Brillant
#0014	Nigeria	0.864	6.54 × 5.15 × 3.15	Light greenish blue	Oval-Brillant
#0016	Mozambique	0.352	5.41 × 3.79 × 2.54	Bluish green	Oval-Brillant
#0019	Mozambique	1.278	9.26 × 4.69 × 3.59	Light bluish green	Cushion-Brillant
#0020	Nigeria	1.526	8.82 × 5.97 × 4.67	Light purplish blue	Pear-Brillant
#0022	Nigeria	0.627	5.36 × 4.76 × 3.77	Yellowish green	Oval-Brillant
#0023	Nigeria	0.190	5.82 × 3.21 × 1.62	Light greenish blue	Pear-Brillant
#0025	Nigeria	0.269	5.09 × 3.89 × 2.43	Light greenish blue	Pear-Brillant
#0033	Mozambique	2.618	8.38 × 8.50 × 4.11	Bluish green	Round-Brillant
#0044	Mozambique	0.903	6.72 × 5.23 × 3.63	Light bluish green	Oval-Brillant
#0050	Mozambique	3.424	11.63 × 8.59 × 4.11	Bluish green	Pear-Brillant
#0063	Brazil	0.219	4.49 × 3.17 × 2.29	Greyish blue green	Oval-Brillant

All samples were examined under a 6 W ultraviolet (UV) lamp (Vilber Lourmat VL-6.LC) with long-wave (365 nm) and short-wave (254 nm) ultraviolet light. Raman spectra were acquired in the 100–1500 cm^{-1} region, during 10 accumulations and 30 s of exposure time, with a Renishaw inVia spectrometer (Renishaw plc, Wotton-under-Edge, Gloucestershire, UK), coupled with an optical microscope and a 514 nm laser excitation (diode-pumped solid-state laser). The laser power on the sample was 4 mW for these spectra, and the spectral resolution was about 2 cm^{-1}. Raman spectra for the region 3000–3800 cm^{-1} were collected with 20 accumulations and a 15 s exposure time. For the PL spectra (520–900 nm), 1 accumulation and 10 s of exposure time with 1 mW laser power were used on the sample. A diamond was used for the calibration of the spectrometer for both Raman and PL measurements by considering its 1331.8 cm^{-1} Raman band. Spectra of three different crystallographic orientations were acquired; the samples were oriented using a polarizer and a conoscope. No polarizer was used during the Raman measurements; thus, in this work, when we talk about different orientations, we refer to different orientations between the incident laser polarization and the *c*-axes of the gems. Visible near-infrared (Vis-NIR) spectra were acquired from 365 to 1000 nm using a mobile instrument (0.05 to 0.10 s acquisition time and 50 accumulations) with an integrating sphere (Gemmosphere, Magilabs Oy (Ltd.), Helsinki, Finland). Thus, Vis-NIR spectra are acquired in a random orientation. For chemical analysis with EDXRF (energy dispersive X-ray fluorescence; Thermo Fisher Scientific Inc., Waltham, MA, USA), sample holders with an aperture diameter of 5 mm were used, and specific sets of parameters were optimized for the most accurate analysis of tourmaline. Various conditions were used for filters and voltage (no filter/4 kV, cellulose/8 kV, aluminum/12 kV, thin palladium/16 kV, medium palladium/20 kV, thick palladium/28 kV, and thick copper/50 kV), with an acquisition time of about 20 min for each sample. All measured iron was calculated as FeO. EDXRF is not an accurate method to measure Na. Moreover, B, Li, F, and water cannot be measured with this method. For this reason, B_2O_3 was fixed at 11%, Li_2O at 3%, H_2O at 4%, and F at 1% for every measurement.

3. Results and Discussion

Fifteen gem quality tourmalines were analyzed with EDXRF in order to obtain the chemical composition of the samples. The obtained data are reported in Table 2 in oxide %. Some of the results discussed in the following sections were obtained considering chemical compositions in atomic %; these data were normalized following the normalization procedure 1 described in Appendix 5 of Henry et al. [1], i.e., fixing at 29 the number of O atoms. Thanks to this approach, the primary tourmaline group for each sample can be identified. Li is fixed as the dominant element in Y-sites (∼1.8 a.p.f.u. for each sample). We closed the X-site occupation, i.e., the sum Na + K + Ca + X-vacant, to 1 a.p.f.u. and

plotted the ternary system for the primary tourmaline group reported in Figure 2. All our analyzed samples except #0044 belong to the alkali group and can be classified as elbaite. Sample #0044 has a higher Ca content (0.6 a.p.f.u.); therefore, it belongs to the calcic group and to the liddicoatite species. As mentioned above, EDXRF analysis is not accurate for measuring Na; thus, these results should be considered with caution. Moreover, F cannot be measured with this method, so the separation between fluor-elbaite and elbaite cannot be performed. The studied samples contain various copper concentrations; in sample #0001, copper content is below the detection limit of the instrument, and sample #0002 presents 1.440% of CuO. These two samples also present relatively high FeO with sample #0025 presenting iron content below the detection limit. The samples are also presenting different contents of Ti, V, Cr, Mn, Zn, Ga, Pb, and Bi (see again Table 2).

All the studied samples were analyzed under UV light. It has been mentioned that long-wave UV light might be used for elbaite-liddicoatite identification since the second tourmaline species typically presents stronger fluorescence under UV than Cu-bearing elbaite due to its higher REE content [9]. However, it was recently discovered that not all Cu-bearing liddicoatite presents strong greenish fluorescence under long-wave UV [15]. Solely sample #0013 presents intense green luminescence under LWUV and faint under SWUV, while 14 out of 15 samples are inert under UV. Thus, it appears that luminescence under UV lamps may not be conclusive for identifying elbaite from liddicoatite.

Vis-NIR spectroscopy is a useful tool to identify Paraíba-type tourmalines [2,10,15,16]. In fact, Cu-bearing tourmalines are characterized by two strong absorption bands around 700 nm and 900 nm, with the second one predominant over the first due to Cu^{2+}, while Fe-rich tourmalines have only an intense band at 720 nm due to Fe^{2+}, sometimes along with a large band at around 520 nm and a couple of sharp bands at around 415 nm due to Mn^{3+} and Mn^{2+}, respectively [12,13]. Figure 3 shows the Vis-NIR spectra for all the tourmalines studied in this work, where for two samples (#0001 and #0002) mainly a strong absorption band around 720 nm due to Fe^{2+} is observed. It is noteworthy that sample #0002 presented the highest content of copper. Under an optical microscope, this sample presented platelets (also observed in Figure 1) previously described as those of native copper [21–24]. The relatively high content of copper is most likely linked to the inclusions; it does not participate in the sample's coloration, and this is mainly due to iron. Thus, this tourmaline cannot be considered the Paraíba type even if the copper content is high as the copper should be the main colorant. For the other thirteen samples, absorptions at about 700 and 900 nm are observed with various relative intensities [25]. These bands are also dependent on the crystallographic direction [3,25]; however, in our measurements, the spectra were acquired in a random orientation.

We studied the behavior of the relative values of the absorbance at 900 nm and 700 nm (A_{900}/A_{700}) in randomly oriented spectra related to the relative Cu and Fe abundance (Cu/(Cu+Fe)) obtained from EDXRF analysis. In Figure 4, two clusters are clearly visible: the first one contains samples with Cu/(Cu+Fe) > 0.5 and $A_{900}/A_{700} > 1$, while the second contains samples with Cu/(Cu+Fe) < 0.5 and $A_{900}/A_{700} < 1$. This might be useful to separate the Paraíba-type tourmalines from tourmalines of similar color, which cannot be considered Paraíba-type tourmalines. For instance, the samples #0001, #0002, #0012, and #0022 cannot be considered Paraíba-type tourmalines. A critical issue, though, is with iron-rich copper-bearing tourmaline. It has been suggested that the samples showing in the o-ray polarized spectrum (obtained by UV-Vis-NIR spectrometer) an absorption band at 700 nm higher than the 900 nm absorption band (related to Cu) is not called Paraíba-type tourmaline [25]. In our study, the samples #0013, #0044, and #0063 are showing absorption intensities related to Fe and Cu of similar intensity (see again Figure 3). We are proposing that only samples with Cu/(Cu+Fe) > 0.6 and $A_{900}/A_{700} > 1.1$ (in randomly oriented spectra) can qualify as Paraíba-type tourmalines.

Table 2. Tourmaline compositions in oxide % obtained with EDXRF analysis and calculated sites occupation in apfu.

Sample	#0001	#0002	#0012	#0013	#0014	#0016	#0019	#0020	#0022	#0023	#0025	#0033	#0044	#0050	#0063
Na_2O	3.73(6)	2.20(8)	2.24(7)	2.78(10)	1.96(6)	2.76(8)	4.16(7)	3.01(6)	2.54(7)	1.42(8)	1.41(8)	3.70(7)	1.74(6)	3.92(6)	3.061(8)
MgO	0.65(2)	1.11(3)	0.81(2)	1.12(3)	0.75(2)	1.13(3)	0.62(2)	0.59(2)	0.85(2)	0.43(2)	0.45(2)	0.55(2)	0.64(2)	0.57(2)	1.06(3)
Al_2O_3	36.30(6)	34.10(7)	36.53(7)	36.46(10)	36.90(7)	34.57(7)	34.44(6)	38.84(6)	35.82(7)	33.57(8)	33.90(8)	35.38(6)	33.00(7)	36.00(6)	34.84(8)
SiO_2	36.69(8)	36.40(10)	38.73(10)	37.3(2)	38.84(9)	37.0(1)	36.36(8)	37.77(8)	38.68(10)	41.8(1)	42.4(1)	36.77(8)	37.69(10)	36.54(7)	36.4(1)
K_2O	0.014(1)	0.040(2)	0.050(2)	0.114(4)	0.040(2)	0.056(3)	0.025(1)	0.018(1)	0.089(4)	0.048(3)	0.053(3)	0.027(1)	0.074(2)	0.016(2)	0.120(4)
CaO	0.251(3)	0.328(4)	0.543(6)	0.802(9)	0.896(7)	0.613(6)	0.199(3)	0.352(4)	0.716(6)	1.30(1)	1.31(1)	0.236(3)	3.87(1)	0.051(2)	0.473(6)
TiO_2	0	0.128(3)	0.014(1)	0.008(2)	0.0015(7)	0.062(3)	0.032(2)	0	0.021(2)	0.001(1)	0	0.048(2)	0.031(2)	0.018(1)	0.023(2)
V_2O_3	0	0.003(1)	0.0015(7)	0	0	0	0.0017(8)	0	0	0	0	0.0013(8)	0	0	0.002(1)
Cr_2O_3	0	0	0	0	0	0	0	0	0	0	0	0.0014(6)	0	0	0.031(1)
MnO	0.502(5)	1.69(1)	0.336(5)	1.44(1)	1.149(7)	3.64(2)	4.94(1)	0.182(3)	0.418(5)	1.47(1)	0.675(8)	3.91(1)	3.14(1)	3.65(1)	3.17(1)
FeO	2.713(9)	3.36(1)	1.321(8)	0.012(3)	0.025(2)	0.139(5)	0	0.024(1)	1.433(8)	0.014(3)	0	0.014(3)	0.082(4)	0.025(3)	0.465(7)
CuO	0	1.440(4)	0.126(1)	0.446(3)	0.271(2)	0.762(3)	0.115(1)	0.151(1)	0.122(1)	0.547(3)	0.481(3)	0.315(2)	0.512(2)	0.158(1)	0.714(3)
ZnO	0.130(1)	0.133(1)	0.226(1)	0.309(2)	0.0042(3)	0.106(1)	0.0014(2)	0.0035(2)	0.215(1)	0.140(1)	0.0031(4)	0.0013(2)	0.0014(3)	0	0.469(2)
Ga_2O_3	0.0170(3)	0.0107(5)	0.0188(5)	0.0220(7)	0.0221(4)	0.0198(5)	0.0552(6)	0.0197(4)	0.0205(5)	0.0241(7)	0.0206(6)	0.0363(5)	0.0541(7)	0.0425(5)	0.0247(6)
PbO	0.0085(2)	0.0140(4)	0.0360(5)	0.118(1)	0.0795(6)	0.0059(3)	0.0059(3)	0.0198(4)	0.0382(5)	0.179(1)	0.202(1)	0.0034(2)	0.0530(6)	0.0012(1)	0.0101(4)
Bi_2O_3	0	0.0536(6)	0.0289(4)	0.0288(6)	0.0600(6)	0.0956(7)	0.0565(5)	0.0188(3)	0.0302(4)	0.0463(7)	0.0670(8)	0.0177(3)	0.1056(7)	0.0055(2)	0.1780(8)
X site															
Na	1.076	0.641	0.637	0.797	0.557	0.799	1.212	0.854	0.725	0.403	0.397	1.072	0.506	1.135	0.891
K	0.003	0.008	0.009	0.022	0.007	0.011	0.005	0.003	0.017	0.009	0.010	0.005	0.014	0.003	0.023
Ca	0.040	0.053	0.086	0.127	0.141	0.098	0.032	0.055	0.113	0.204	0.205	0.038	0.622	0.008	0.076
vacancy	0	0.298	0.268	0.054	0.295	0.092	0	0.088	0.145	0.384	0.388	0	0	0	0.010
T site															
Si	5.463	5.484	5.692	5.527	5.696	5.542	5.470	5.524	5.703	6.128	6.187	5.497	5.652	5.454	5.460
Al	0.537	0.516	0.308	0.473	0.304	0.458	0.530	0.476	0.297	0	0	0.503	0.348	0.546	0.540
Z+Y sites															
Al	6.166	5.807	6.328	6.261	6.377	5.948	5.851	6.662	6.225	5.800	5.827	6.043	5.787	6.105	5.911
Li	1.796	1.818	1.773	1.786	1.769	1.805	1.815	1.765	1.779	1.768	1.759	1.803	1.809	1.801	1.811
Fe	0.338	0.423	0.162	0.001	0.003	0.017	0	0.003	0.177	0.002	0	0.002	0.010	0.003	0.058
Cu	0	0.164	0.014	0.050	0.030	0.086	0.013	0.017	0.014	0.061	0.053	0.036	0.058	0.018	0.081
Mn	0.063	0.215	0.042	0.181	0.143	0.461	0.629	0.023	0.052	0.183	0.083	0.495	0.399	0.461	0.403
Mg	0.144	0.25	0.177	0.248	0.164	0.253	0.139	0.128	0.188	0.094	0.097	0.121	0.143	0.127	0.236
Ti	0	0.015	0.002	0.001	0.001	0.007	0.004	0	0.002	0.001	0	0.005	0.003	0.002	0.003
Zn	0.014	0.015	0.025	0.034	0.001	0.012	0.001	0.001	0.023	0.015	0.001	0.001	0.001	0	0.052
V	0	0.0004	0.0002	0	0	0	0.0002	0	0	0	0	0.0001	0	0	0.0002
Cr	0	0	0	0	0	0	0	0	0	0	0	0.0001	0	0	0.004
Ga	0.00163	0.00103	0.00178	0.00209	0.00208	0.0019	0.00533	0.00184	0.00194	0.00227	0.00192	0.00348	0.00524	0.00407	0.00235
Pb	0.0003	0.0006	0.001	0.005	0.003	0.0002	0.0002	0.001	0.002	0.007	0.008	0.0001	0.002	0.0001	0.0004
Bi	0	0.002	0.001	0.001	0.002	0.004	0.002	0.0007	0.001	0.002	0.003	0.0007	0.004	0.0002	0.007

Table 2. *Cont.*

Sample	#0001	#0002	#0012	#0013	#0014	#0016	#0019	#0020	#0022	#0023	#0025	#0033	#0044	#0050	#0063
V site															
OH	3.000	3.000	3.000	3.000	3.000	3.000	3.000	3.000	3.000	3.000	3.000	3.000	3.000	3.000	3.000
W site															
OH	0.972	1.020	0.922	0.951	0.9126	0.992	1.014	0.903	0.934	0.911	0.891	0.988	1.001	0.982	1.006
F	0.256	0.259	0.252	0.254	0.2518	0.257	0.258	0.251	0.253	0.252	0.250	0.257	0.257	0.256	0.258

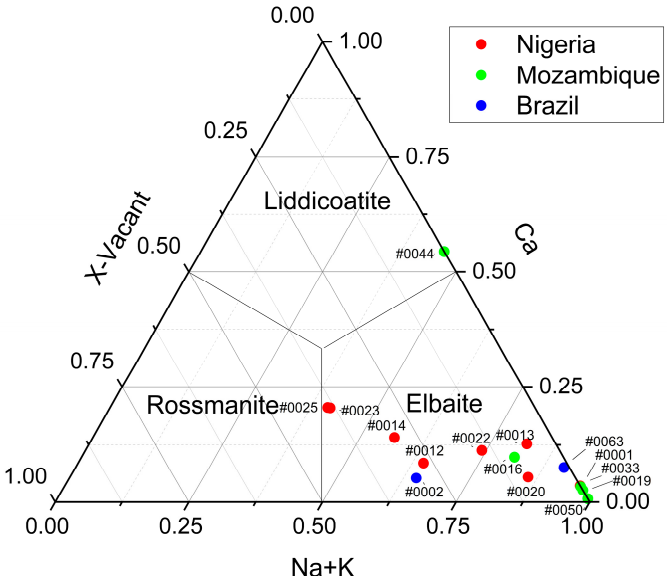

Figure 2. Ternary system for primary tourmaline groups depending on X-site occupancy. For alkali group tourmalines, we have elbaite; for the calcic group, we have liddicoatite; and for the X-site vacant group, we have rossmanite. Only sample #0044 is in the liddicoatite region; all the other samples are elbaite.

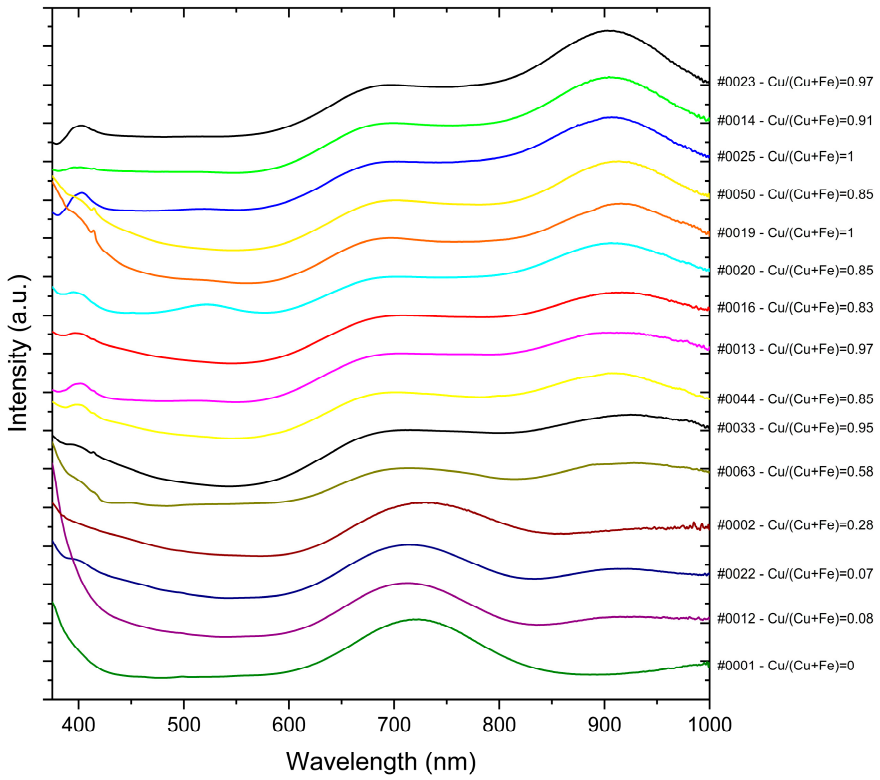

Figure 3. Vis-NIR absorption spectra for all the samples analyzed in this work. Cu-bearing tourmalines (spectra at the top) present both bands at 700 nm and 900 nm, while Fe-rich tourmalines (spectra at the bottom) have only one band around 720 nm. Each spectrum is normalized with respect to the absolute intensity of the 700 nm band.

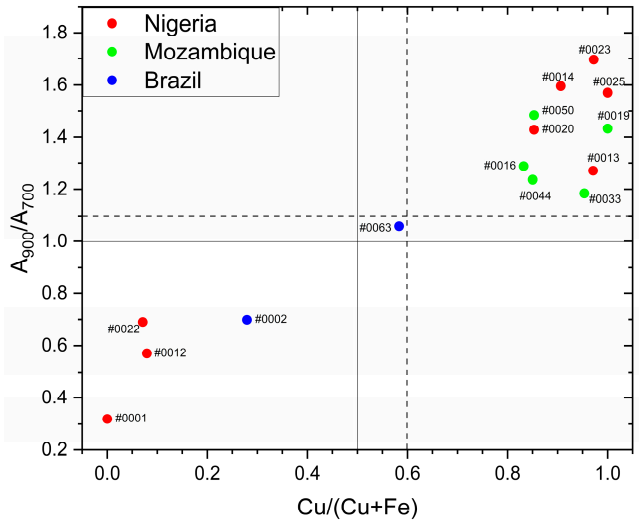

Figure 4. Relative intensities of the two absorption bands at 900 nm and 700 nm depending on the Cu/(Cu+Fe) ratio. Two regions are clearly visible: Cu-bearing tourmalines with A_{900}/A_{700} higher than 1 and Cu/(Cu+Fe) higher than 0.5, as well as Fe-rich tourmalines with A_{900}/A_{700} lower than 1 and Cu/(Cu+Fe) lower than 0.5. However, only tourmalines with Cu/(Cu+Fe) > 0.6 and A_{900}/A_{700} > 1.1 can be considered the Paraíba type.

Photoluminescence spectroscopy was previously used to distinguish between elbaite and liddicoatite thanks to a series of bands in the 850–950 nm region present in the latter species [15,26]. This behavior is confirmed by liddicoatite sample #0044, showing these typical features that are not present in other elbaite samples' PL spectra (Figure 5). Sample #0044 was analyzed in three perpendicular crystallographic orientations in order to verify if these bands can be detected in a random orientation. All three PL spectra in Figure 6 show the same bands, indicating that these features are not polarization-dependent and can always be detected, allowing us to distinguish between liddicoatite and elbaite with PL spectroscopy in a random orientation. These PL spectra bands are most likely linked to the presence of REE and possibly Nd^{3+}, which can substitute for calcium present in the case of liddicoatite tourmalines [27].

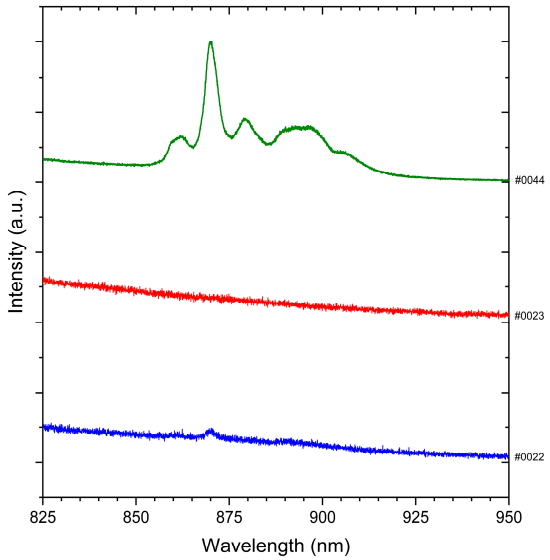

Figure 5. PL spectra in the 825–900 nm region of some of the analyzed samples. Only liddicoatite sample #0044 spectrum (green spectrum) has bands in this region, while other elbaite samples do not show any features (e.g., red spectrum). Only the #0022 elbaite (blue spectrum) sample exhibits a weak peak at 870 nm.

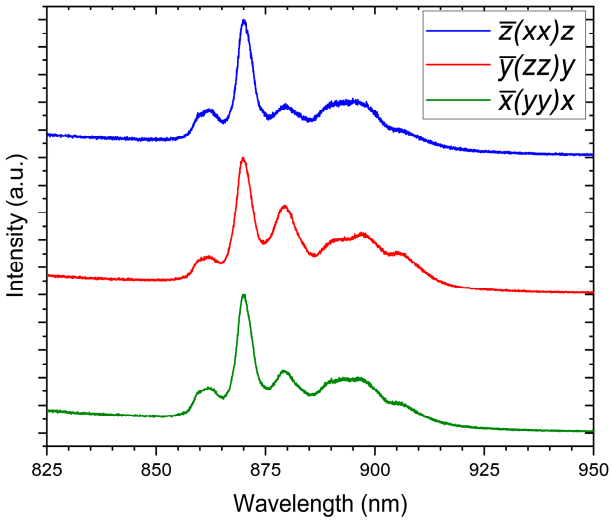

Figure 6. PL spectra in the 825–900 nm region of sample #0044 in three perpendicular orientations (in the red spectrum, the incident light is polarized parallel to the *c*-axis of the crystal); typical REE (possibly Nd^{3+}) bands are visible in all the three spectra.

Raman spectra were collected from all the samples with different crystallographic orientations to check the possibility of distinguishing elbaite from liddicoatite tourmalines in random orientations. Both Raman spectra from 200 to 1200 cm^{-1} (fingerprint region) and from 3250 to 3800 cm^{-1} (OH stretching region) were analyzed. In Figure 7, a spectrum for every sample in a random orientation is presented. It appears that elbaite and liddicoatite can be distinguished thanks to the peaks' positions in the OH stretching region, as previously mentioned [15,16]. Elbaite shows two main peaks at 3484 ± 5 cm^{-1} and 3593 ± 2 cm^{-1}, while in liddicoatite the main peak is located at 3610 ± 1 cm^{-1} with a less intense peak located at 3508 ± 2 cm^{-1}. Only the #0044 sample shows liddicoatite's typical peaks, while all the other samples have Raman spectra of elbaite, in agreement with the results obtained from EDXRF and PL spectroscopy previously discussed. Some of the elbaite gems show an additional band at 3560 cm^{-1}, which is particularly evident in samples #0001 and #0002. This band is due to the presence of iron in the Y site, as confirmed by EDXRF analysis, in a configuration with prevalent Fe and secondary Al in the Y sites and Al in the Z sites [16].

The OH bands' positions seem to be independent from orientation; in fact, with changing crystal orientation, only changes in relative intensities were detected in both elbaite and liddicoatite (Figure 8A,B). In the fingerprint region, the behavior is more complicated: peak positions are strongly dependent on crystal orientation; for example, the main peak above 700 cm^{-1}, related to SiO_4 tetrahedra stretching modes, has a shift in its position from 710 cm^{-1} to 730 cm^{-1} in both elbaite and liddicoatite samples, depending on orientation. This is related to the polar behavior of tourmalines with longitudinal optical modes (A_1 and E) at higher wavenumbers with respect to correspondent transverse optical modes, as described in references [16,28,29].

Raman spectra of elbaite and liddicoatite obtained with incident light polarized along the crystal *c*-axis, i.e., in the $\overline{y}(zz)y$ configuration, exhibit distinct characteristics in the 200–300 cm^{-1} region. Elbaite (such as sample #0063) usually presents three peaks with decreasing intensities (Figure 8B, black spectrum), with wavenumbers in the ranges 222 ± 1, 246 ± 1, and 271 ± 3 cm^{-1}. On the other hand, liddicoatite (sample #0044) shows two partially overlapped peaks with similar intensities (Figure 8A, black spectrum). The peaks in this region are related to the YO_6 octahedra vibrational modes [29]; however, since no compositional difference in Y sites is expected between elbaite and liddicoatite, YO_6 vibrational modes can be influenced by the anionic X site occupation. This region can be used to identify elbaite and liddicoatite only if gems are analyzed in the correct crystallographic orientation. In different orientations, this region presents different peaks

in both liddicoatite and elbaite that are like each other and that make it challenging to distinguish between the two species (Figure 8A,B, blue and red spectra).

On the other hand, few differences for the positions of the bands situated in OH stretching region are present. These vibrational modes are divided into ^{V}OH modes (3400–3615 cm^{-1}), related to the stretching of OH groups in V sites, and ^{W}OH modes (3615–3820 cm^{-1}), related to the stretching of the OH group in the W site, but both can be influenced by the X, Y, and Z site occupancy [16]. Liddicoatite tourmaline presents the main Raman band slightly above 3600 cm^{-1} and elbaite tourmaline slightly below 3600 cm^{-1} regardless the crystallographic orientation (see again Figure 8). Thus, it appears that bands in the OH stretching region are the best indicators for elbaite and liddicoatite identification with Raman spectroscopy in random crystallographic orientation, while the fingerprint region can only give information on tourmaline species if they are analyzed in the $\overline{y}(zz)y$ configuration.

We also searched for possible correlations between changes in peak parameters and variations in the Cu/(Cu+Fe) ratio in order to evaluate the applicability of Raman spectroscopy for the identification of Paraíba-type tourmalines. No relations were found though with any parameter. Only a band at 3560 cm^{-1} in the OH region appeared in the Fe-rich samples.

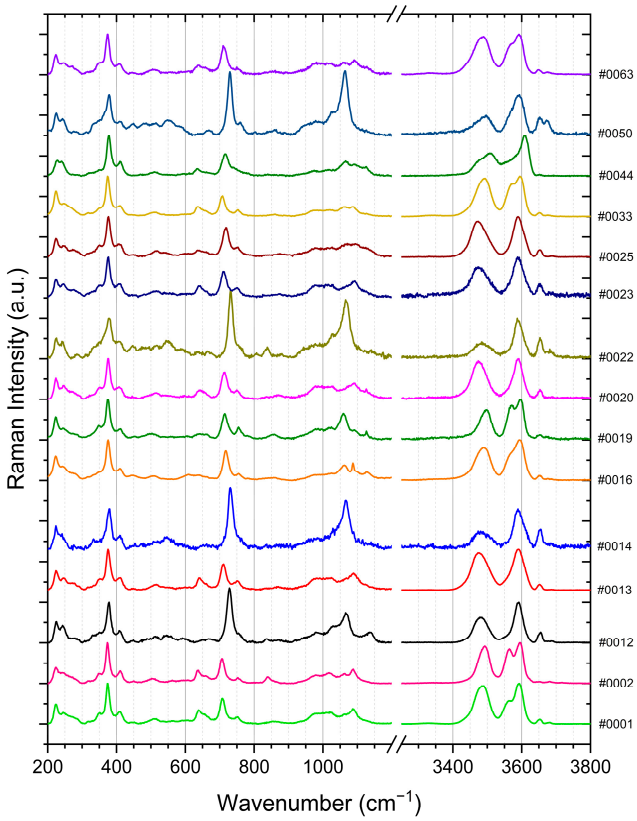

Figure 7. Normalized Raman spectra of all the analyzed samples in both the fingerprint and OH stretching regions. Liddicoatite (#0044) can be distinguished from elbaite (all the other spectra) by peak positions in the OH region. Spectra intensities are normalized with respect to the absolute intensity of the ~370 cm^{-1} peak in the fingerprint region, while those in the OH region are normalized with respect to the absolute intensity of the main peak (i.e., the peak at ~3593 cm^{-1} in elbaite and the one at ~3610 cm^{-1} in liddicoatite).

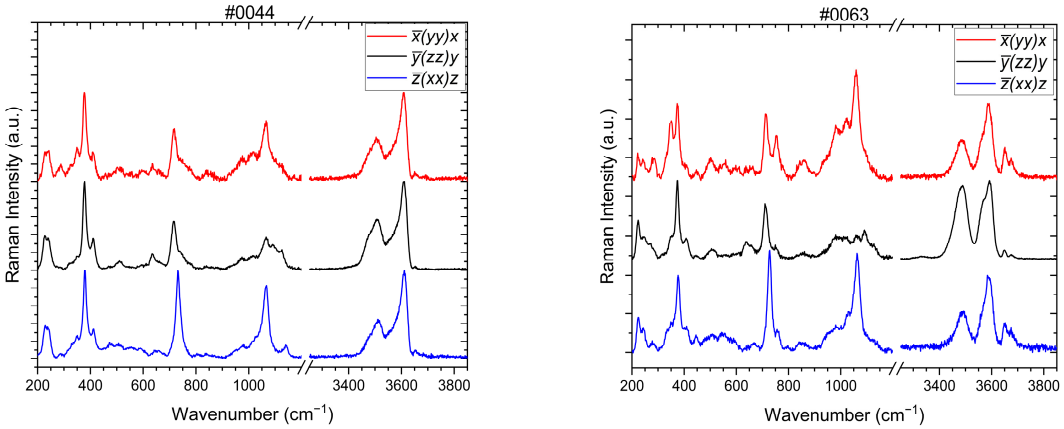

(**A**) (**B**)

Figure 8. Liddicoatite (**A**) and elbaite (**B**) normalized Raman spectra measured in three perpendicular crystallographic orientations. For peaks in the OH stretching region, only absolute and relative intensities change depending on orientation, without any shift in peak positions. In the fingerprint region, the behavior is more complicated, with different modes activated depending on crystal orientation for both tourmaline species. The intensities of the spectra here represented are normalized with respect to the absolute intensity of the ~370 cm^{-1} peak in the fingerprint region, while those in the OH region are normalized with respect to the absolute intensity of the main peak (i.e., the peak at ~3593 cm^{-1} in elbaite and the one at ~3610 cm^{-1} in liddicoatite).

4. Conclusions

A multi-methodological investigation of different blue to green gem-quality Li-tourmaline samples has been performed, focusing in particular on results obtained from Raman spectroscopy in random crystallographic orientations. It has been found that OH stretching mode positions are different in elbaite and liddicoatite and are not dependent on crystal orientation. Results obtained from EDXRF and Vis-NIR confirm previous results from the literature, and they agree with data obtained from Raman spectroscopy, highlighting the potential applicability of OH peak positions to distinguish between elbaite and liddicoatite. The fingerprint region of the Raman spectrum can be used for elbaite-liddicoatite identification only if obtained in the $\bar{y}(zz)y$ configuration, while in other crystallographic orientations, the vibrational modes are located in similar positions in both tourmaline species. PL spectroscopy and the pronounced REE-related bands in the NIR present in liddicoatite samples can be further used to help in the separation between the tourmaline species. No correlation between Raman parameters and Cu content was found, thus Raman spectroscopy cannot be used to determine if a tourmaline is the Paraíba type or not. A suggested method to separate Paraíba-type tourmalines from tourmalines of similar color that cannot be called the Paraíba type is using EDXRF data and unoriented Vis-NIR spectra drawing the limits at Cu/(Cu+Fe) = 0.6 and A_{900}/A_{700} = 1.1. However, additional samples need to be studied in order to further confirm the findings presented in this paper.

Author Contributions: Investigation, L.B., U.H. and S.K.; formal analysis, L.P. and D.B.; methodology, S.A. and J.S.; writing-original draft preparation: L.P., S.K. and D.B. All authors have read and agreed to the published version of the manuscript.

Funding: This research received no external funding.

Data Availability Statement: Data are contained within the article.

Conflicts of Interest: The authors declare no conflicts of interest.

References

1. Henry, D.J.; Novák, M.; Hawthorne, F.C.; Ertl, A.; Dutrow, B.L.; Uher, P.; Pezzotta, F. Nomenclature of the Tourmaline-Supergroup Minerals. *Am. Mineral.* **2011**, *96*, 895–913. [CrossRef]

2. Pezzotta, F.; Laurs, B.M. Tourmaline: The Kaleidoscopic Gemstone. *Elements* **2011**, *7*, 333–338. [CrossRef]
3. Fritsch, E.; Shigley, J.E.; Rossman, G.R.; Mercer, M.E.; Muhlmeister, S.M.; Moon, M. Gem-Quality Cuprian-Elbaite Tourmalines from São José de Batalha, Paraíba, Brazil. *Gems Gemol.* **1990**, *26*, 189–205. [CrossRef]
4. Abduriyim, A.; Kitawaki, H.; Furuya, M.; Schwarz, D. "Paraiba"-Type Copper-Bearing Tourmaline Form Brazil, Nigeria, and Mozambique: Chemical Fingerprint by LA-ICP-MS. *Gems Gemol.* **2006**, *42*, 4–21. [CrossRef]
5. LMHC Standardised Gemmological Report Wording LMHC Information Sheet #6. Available online: https://www.lmhc-gemmology.org/wp-content/uploads/2023/06/LMHC-Information-Sheet_6_V8_2023.pdf (accessed on 5 October 2023).
6. Shigley, J.E.; Cook, B.C.; Laurs, B.M.; de Oliveira Bernardes, M. An Update on "Paraíba" Tourmaline from Brazil. *Gems Gemol.* **2001**, *37*, 260–276. [CrossRef]
7. Okrusch, M.; Ertl, A.; Schüssler, U.; Tillmanns, E.; Brätz, H.; Bank, H. Major- and Trace-Element Composition of Paraíba-Type Tourmaline from Brazil, Mozambique and Nigeria. *J. Gemmol.* **2016**, *35*, 120–139. [CrossRef]
8. Karampelas, S.; Klemm, L. "Neon" Blue-to-Green Cu-and Mn-Bearing Liddicoatite Tourmaline. *Gems Gemol.* **2010**, *46*, 323–325.
9. Katsurada, Y.; Sun, Z. Cuprian Liddicoatite Tourmaline. *Gems Gemol.* **2017**, *53*, 34–41. [CrossRef]
10. Katsurada, Y.; Sun, Z.; Breeding, C.M.; Dutrow, B.L. Geographic Origin Determination of Paraíba Tourmaline. *Gems Gemol.* **2019**, *55*, 648–659. [CrossRef]
11. Ertl, A.; Giester, G.; Schüssler, U.; Brätz, H.; Okrusch, M.; Tillmanns, E.; Bank, H. Cu- and Mn-Bearing Tourmalines from Brazil and Mozambique: Crystal Structures, Chemistry and Correlations. *Miner. Pet.* **2013**, *107*, 265–279. [CrossRef]
12. Merkel, P.B.; Breeding, C.M. Spectral Differentiation Between Copper and Iron Colorants in Gem Tourmalines. *Gem Gemol.* **2009**, *45*, 112–119. [CrossRef]
13. Laurs, B.M.; Zwaan, J.C.; Breeding, C.M.; Simmons, W.B.; Beaton, D.; Rijsdijk, K.F.; Befi, R.; Falster, A.U. Copper-Bearing (Paraiba-Type) Tourmaline from Mozambique. *Gems Gemol.* **2008**, *44*, 294–320. [CrossRef]
14. Sun, Z.; Palke, A.C.; Breeding, C.M.; Dutrow, B. A New Method for Determining Gem Tourmaline Species by LA-ICP-MS. *Gems Gemol.* **2019**, *55*, 2–17. [CrossRef]
15. Hennebois, U.; Delaunay, A.; Karampelas, S. Separating Elbaite from Liddicoatite Paraiba-Type Tourmaline. *J. Gemmol.* **2022**, *38*, 317–319. [CrossRef]
16. Watenphul, A.; Burgdorf, M.; Schlüter, J.; Horn, I.; Malcherek, T.; Mihailova, B. Exploring the Potential of Raman Spectroscopy for Crystallochemical Analyses of Complex Hydrous Silicates: II. Tourmalines. *Am. Mineral.* **2016**, *101*, 970–985. [CrossRef]
17. Van Hinsberg, V.J.; Henry, D.J.; Marschall, H.R. Tourmaline: An Ideal Indicator of Its Host Environment. *Can. Miner.* **2011**, *49*, 1–16. [CrossRef]
18. Hawthorne, F.C.; Dirlam, D.M. Tourmaline the Indicator Mineral: From Atomic Arrangement to Viking Navigation. *Elements* **2011**, *7*, 307–312. [CrossRef]
19. Musiyachenko, K.A.; Korsakov, A.V.; Shimizu, R.; Zelenovskiy, P.S.; Shur, V.Y. New Insights on Raman Spectrum of K-Bearing Tourmaline. *J. Raman Spectrosc.* **2020**, *51*, 1415–1424. [CrossRef]
20. Korsakov, A.V.; Rezvukhina, O.V.; Rezvukhin, D.I.; Greshnyakov, E.D.; Shur, V.Y. Dumortierite and Tourmaline from the Barchi-Kol Diamond-Bearing Kyanite Gneisses (Kokchetav Massif): A Raman Spectroscopic Study and Petrological Implications. *J. Raman Spectrosc.* **2020**, *51*, 1839–1848. [CrossRef]
21. Krzemnicki, M.S.; Wang, H.A.O. Paraiba or Not? Cu-Bearing Tourmaline with a Distinct Fe Concentration. *J. Gemmol.* **2022**, *38*, 20–22. [CrossRef]
22. Brandstatter, F.; Niedermayr, G. Copper and Tenorite Inclusions in Cuprian-Elbaite Tourmaline from Paraiba, Brazil. *Gems Gemol.* **1994**, *30*, 178–183. [CrossRef]
23. Hartley, A. Native Copper Inclusions in a Cu-Bearing Tourmaline. *J. Gemmol.* **2018**, *36*, 203.
24. Wang, H.A.O.; Grolimund, D.; Franz, L.; Mathys, D.; Schultz-Güttler, R.; Krzemnicki, M.S. Further Characterisation of Native Copper Inclusions In-Bearing Tourmaline. *J. Gemmol.* **2023**, *38*, 427–429. [CrossRef]
25. Rossman, G.R.; Fritsch, E.; Shigley, J.E. Origin of Color in Cuprian Elbaite from São José de Batalha, Paraíba, Brazil. *Am. Mineral.* **1991**, *76*, 1479–1484.
26. Milisenda, C.C.; Müller, S. REE Photoluminescence in Paraìba Type Tourmaline from Mozambique. In Proceedings of the 35th International Gemmological Conference, Windhoek, Namibia, 11–15 October 2017; pp. 71–73.
27. Lenz, C.; Nasdala, L.; Talla, D.; Hauzenberger, C.; Seitz, R.; Kolitsch, U. Laser-Induced REE3+ Photoluminescence of Selected Accessory Minerals—An "Advantageous Artefact" in Raman Spectroscopy. *Chem Geol* **2015**, *415*, 1–16. [CrossRef]
28. Alvarez, M.A.; Coy-Yll, R. Raman Spectra of Tourmaline. *Spectrochim. Acta* **1978**, *34*, 899–908. [CrossRef]
29. Watenphul, A.; Schlüter, J.; Bosi, F.; Skogby, H.; Malcherek, T.; Mihailova, B. Influence of the Octahedral Cationic-Site Occupancies on the Framework Vibrations of Li-Free Tourmalines, with Implications for Estimating Temperature and Oxygen Fugacity in Host Rocks. *Am. Mineral.* **2016**, *101*, 2554–2563. [CrossRef]